Journal of Alloys and Compounds 691 (2017) 15–25

Contents lists available at ScienceDirect

Journal of Alloys and Compounds

journal homepage: http://www.elsevier.com/locate/jalcom

Design of Mg alloys: The effects of Li concentration on the structure and elastic properties in the Mg-Li binary system by first principles calculations

Olivia Pavlic [a, *], Wilfredo Ibarra-Hernandez [a], Irais Valencia-Jaime [a, b], Sobhit Singh [a], Guillermo Avendaño-Franco [a], Dierk Raabe [c], Aldo H. Romero [a]

[a] Physics Department, West Virginia University, WV, 26506-6315 Morgantown, USA
[b] Centro de Investigación y Estudios Avanzados del IPN, MX, 76230 Querétaro, Mexico
[c] Max-Planck-Institut für Eisenforschung, Max-Planck-Straße, 1, 40237 Düsseldorf, Germany

ARTICLE INFO

Article history:
Received 23 June 2016
Received in revised form
17 August 2016
Accepted 22 August 2016
Available online 24 August 2016

Keywords:
ab initio calculations
Elastic properties
Magnesium
Lithium
Crystal structure

ABSTRACT

First principles calculations have been employed to search for energetically stable structures of the Mg-Li binary system over all possible Mg concentrations. Volume, space group, c/a and b/a ratios, vibrational contribution to the heat capacity, and Debye temperature are reported to investigate the effects of Li concentration on the Mg-Li binary system. Structures of high symmetry and those lying on or close to the convex hull are further explored to search for dynamic and elastic stability. Five ground state structures were found at Li_1Mg_{13}, Li_1Mg_2, Li_1Mg_1, Li_7Mg_2, and $Li_{15}Mg_1$ compositions. Elastic constants and elastic properties of the selected low energy structures were calculated and analyzed. We also investigate the effect of the phonon band gap found in Li_1Mg_1 and Li_1Mg_2 on lattice thermal conductivity.

1. Introduction

Mg has been studied since the 1950's because of its potential applications as a cost effective and lightweight structural metal [1,2]. It exhibits many desirable qualities including good recyclability, castability, weldability, and high specific strength [3–6]. Additionally, Mg is among the lightest metallic structural materials with a low density of 1.74 g/cm^3. This, along with its natural abundance, makes Mg and its alloys very attractive to industries, especially the aerospace and automobile industries where its application could minimize the environmental impact of their products [7,8]. Currently Mg is not widely used because of the low ductility inherent to its hexagonal close packed (HCP) lattice structure. This inhibition of plastic deformations in HCP Mg has been a topic of extensive study [9–12]. Here we try to overcome this limitation.

One way to improve Mg's ductility is to alloy it with another metal. Recently, alloying Mg by solid solution with rare earth elements has been investigated [13–17]. While these studies focus on the type of alloying element, here we focus on changing the lattice structure from an HCP lattice to a cubic one, the ideal structure for ductile materials. To maintain the lightweight benefits of Mg, we systematically study the influence of body centered cubic (BCC) Lithium (Li) as an alloy because of its low density (0.58 g/cm^3) and cubic structure [4,5,18].

Many groups have approached the Mg-Li system by investigating the properties of few ordered structures. The most common method is to fix the lattice and change the atoms, where only hexagonal and cubic lattice structures are considered. In 2001, Uesugi at al [24]. used the local density approximation within density functional theory to investigate three different configurations for 87% Mg. Counts et al. [25] studied the mechanical properties of cubic supercells of Mg-Li of various Mg concentrations using a generalized gradient approximation within density functional theory. Taylor, Curtarolo, and Hart [26] made predictions of Mg-Li ordered phases using the first-principles-based cluster-expansion (CE) method and found ground states at 12%, 50%, 66%, and 75% Mg concentrations. Liang and Gong [27] selected three Mg-Li compositions and studied the structural stability and elastic properties. They used a generalized gradient first principles approximation to find the crystal structure of the ground state of each composition. Phasha et al. [3] also used density functional

* Corresponding author.
E-mail address: ompavlic@mix.wvu.edu (O. Pavlic).

http://dx.doi.org/10.1016/j.jallcom.2016.08.217
0925-8388/

theory within the generalized gradient approximation to investigate the existence of fcc and bcc structures at 50%, 75%, 83% and 87% Mg concentrations. That group later also studied random Mg-Li alloys in HCP, FCC, and BCC lattices [28]. Shin and Carter [4] applied orbital-free density functional theory (OFDFT) to ordered and disordered bcc Mg-Li supercells to study their elastic properties.

Our study approaches the problem from a new perspective, by beginning with an *ab-initio* energy search over all possible compositions and structures. This allows us to find naturally occurring structures over the complete composition range of the two metals. From the results we then select the most promising structures. Our selection criteria is based on the space group and formation energy of the structure. Foremost, we look for high symmetry structures as it is likely that these will be the structures with the highest ductility. We also choose structures with the lowest formation energy as these are the most stable and therefore the most likely to be able to be synthesized. We then further analyze these favorable structures to investigate and characterize the elastic properties and stability. We have calculated the elastic constants for each structure and have plotted the macroscopic elastic properties: bulk modulus, shear modulus, Young's modulus, poisson ratio and bulk/shear ratio. From these results we can determine the effect Li concentration has on the properties of the system.

In the following, we present a description of the computational details of the methods used to obtain our results. Then a discussion of the predicted structures with emphasis on the ground state structures is given. This is followed by the elastic properties, the heat capacity, thermal conductivity of the lattice of Li_1 Mg_1 and Li_1 Mg_2, and a conclusion which summarizes the findings.

2. Methods

Several numerical techniques have been developed for structure prediction. We use the Minima Hopping Method (MHM) [29–31] to effectively sample the entire potential energy surface and find the global energy minimum. MHM uses a dynamical algorithm with temperature as the variable. A series of consecutive short molecular dynamics simulations are used to overcome energy barriers and 'hop' from local energy minima. Local geometry relaxations follow each hop to identify the configuration corresponding to energy minima. The escape is made efficient by choosing the initial velocities of molecular dynamics trajectories approximately along soft mode directions. We use this method in conjunction with *ab-initio* density functional theory (DFT) to predict stable and metastable structures. The only information required is the chemical composition of the system. For all our structural search calculations, we have used unit cells containing up to 16 atoms with concentrations ranging from 0 to 100% Li. The evaluation of energy and forces were performed using DFT as implemented in the Vienna Ab initio Simulation Package (VASP) [32,33]. The Perdew-Burke-Ernzerhof (PBE) [34] generalized gradient approximation was used for the exchange correlation functional. The k-mesh used to sample the Brillouin zone was converged to guarantee a numerical accuracy of the total energy to less than 2meV/atom and the plane wave cutoff was converged to 550eV. All forces were converged to better than 1 meV/Å. The PHONOPY [35,36] software interfaced with VASP was used to obtain the force constants from VASP using the finite difference approach with a $2 \times 2 \times 2$ supercell. Elastic constants converged to more than 1 GPa were calculated from strain stress relations as implemented in VASP.

For the calculation of the lattice contribution to the thermal conductivity, we perform ab-initio calculations in the framework of Density Functional Theory and Density Functional Perturbation Theory as implemented in the Quantum Espresso package [37] to obtain 2nd-order interatomic force constants (IFCs) from fully relaxed structures. We use the thirdorder.py script [38] provided by ShengBTE code [39], to create perturbed supercells which allows us to accurately estimate 3rd-order IFCs in an ulterior calculation. We take into account interactions up to the fourth neighbor. We determine the lattice contributions to the total thermal conductivity by use of the iterative solution of the Boltzmann transport equation (BTE) for phonons as implemented in the ShengBTE code [39]. This package reads the second and third order interatomic force constants and uses them to solve the BTE for phonons. We can then estimate the phonon velocities and phonon life-times due to phonon-phonon interactions which finally leads to thermal conductivity. To obtain accurate values of the IFCs, we increase the q-point mesh up to $8 \times 8 \times 8$ and $6 \times 6 \times 6$ for Li_1 Mg_1 and Li_1 Mg_2, respectively.

3. Results

To ensure stability of our predicted structures, we do three analyses. First, we review the energetic stability of the structures we have found. To do so, we re-optimize the results of our MHM calculations with tighter energy convergence criteria and find the formation energy. In Fig. 1, we plot these formation energies with respect to Li concentration. Every blue x represents the formation energy of each structure found at the bottom of an energy valley for a particular composition. The solid line at the bottom connects the lowest energy structures and depicts the convex-hull for the Mg-Li system. Any structures which fall on this line, marked by a magenta circle, are energetically stable and can be chemically synthesized. There are three online databases which have reported theoretical results for the Mg-Li system: The Materials Project [19–21] is an online database dedicated to predicting properties of materials, AFLOW [23] is an online library of structural ab initio calculations, and Open Quantum Materials Database (OQMD) [22] is a database of DFT calculated thermodynamic and structural properties. We have included structures from these databases to our results for comparison. Each of these structures from other studies has been reoptomized with our psudopotentials and convergence criteria. We see that our search method has found structures at all the compositions reported by these sources. While we find many of our structures to be of lower energy than the reported ground states, there are three places where our results are of higher formation energy: at the compositions Li_1 Mg_2, Li_2 Mg_1, and Li_3 Mg_1. However, these results are within the numerical accuracy of our calculations. We find five structures on the convex hull, three of which are previously unreported. Each will be discussed in more detail below.

In order to check the thermodynamic stability we calculate the phonon dispersion. It is well known that a positive phonon dispersion indicates thermal stability. Interestingly, we find a phonon gap in a large portion of our structures. The phonon spectra as well as phonon density of states can be found in the supplementary information. We have further investigated the phonon contribution to the specific heat and have used PHONOPY [35,36] to calculate the Debye temperatures for each of the structures on the convex hull. These results will be discussed further below.

Third, we have calculated the elastic stability as outlined in ref 35 [40]. Due to the range of crystal structures we found, we refer the reader to the original work for a detailed description of the calculations. All of the structures presented in Table 1 meet this elastic stability criteria.

To see how Li concentration affects the crystal lattice, in Fig. 2 we plot the space group of the lowest energy structure and the highest symmetry stucture, a histogram of the number of stuctures found in each spacegroup overall, and the convex hull with symbols indicative of the space group of each structure. From the histogram

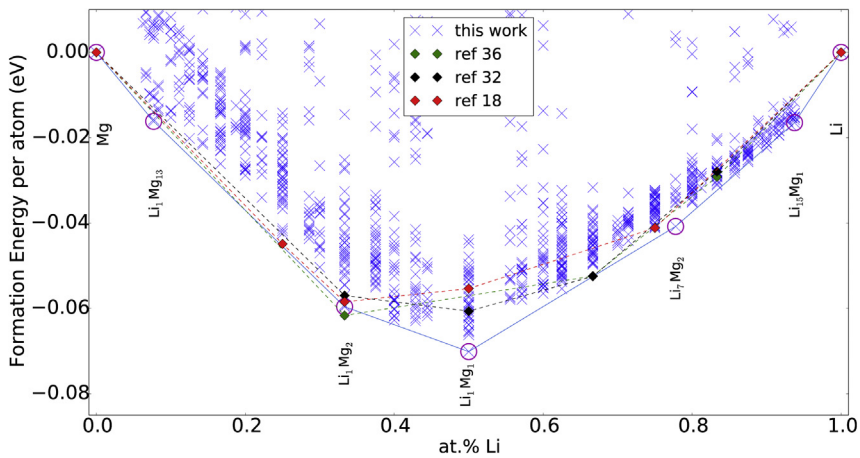

Fig. 1. Convex hull of the Li-Mg Binary system. Blue x's indicate structures from this work, where magenta circles indicate structures belonging to the convex hull. Green diamons are stuctures from The Materials Project [19–21], black diamonds are structures from the Open Quantum Materials Database [22], and red diamonds are structures obtained from the AFLOW online database [23]. (For interpretation of the references to colour in this figure legend, the reader is referred to the web version of this article.)

Table 1
Space group, number of atoms in the primitive cell and formation energy for structures close to the convex hull.

% Li	Phase	Space group	Atoms in primitive cell	Formation Energy (meV)
7	Li_1 Mg_{13}	*P*1 (1)	14	−9.7 (ground)
25	Li_1 Mg_3	*Fm*-3*m* (225)	4	−27.6 (metastable)
33	Li_1 Mg_2	*P*-6*m*2 (187)	3	−35.5 (metastable)
33	Li_1 Mg_2	*I*4/*mmm* (139)	3	−59.6 (ground)
40	Li_2 Mg_3	*R*-3*m* (166)	5	−62.7 (ground)
43	Li_3 Mg_4	*P*6/*mmm* (191)	7	−15.6 (metastable)
50	Li_1 Mg_1	*Pm*-3*m* (221)	2	−70.1 (ground)
50	Li Mg_1	*P*4/*mmm* (123)	2	−65.2 (metastable)
78	Li_7 Mg_2	*Immm* (71)	9	−40.7 (ground)
84	Li_5 Mg_1	*P*-62*m* (189)	6	−28.0 (metastable)
85	Li_6 Mg_1	*P*1 (1)	7	−28.3 (ground)
88	Li_7 Mg_1	*P*-6*m*2 (187)	8	−24.2 (metastable)
90	Li_9 Mg_1	*C*12/*m*1 (12)	10	−22.3 (ground)
93	Li_{15} Mg_1	*Cmmm* (65)	16	−16.4 (ground)

we see an overwhelming majority of stuctures are of low symmetry. In Fig. 3 we plot the c/a and b/a ratios with respect to at.% Lithium. We include values for the ground state structure and the highest symmetry structure for each composition. We also plot the volume with respect to at.% Lithium.

It is important at this point to note that because of the richness of lattice symmetry in our results, comparison of our results with previous works present in the literature proves challenging. All studies found in the literature concern only hexagonal and cubic structures, with the exception of the results of ref 3 [3]. The databases do not show this exclusion of lower symmetry structures. The results of Taylor et al. can be found in ref 26 [26] as well as on the online database, AFLOW [23]. AFLOW includes structures of lower symmetry than cubic and hexagonal, while the only results that are analyzed in ref 26 are those which are cubic and hexagonal. Experimentally, these are the lattice types which are found [18,41–43] and so are those which theoretical calculations are based upon. However, our structural search is able to locate a large diversity of crystal symmetries, which indicates the richness of the Mg-Li compounds. In Fig. 2 we see that there are only a small number of cubic and hexagonal structures, but many of tetragonal symmetry. We can find in ref 3 [3] the inclusion of tetragonal structures. Since our calculations are performed at zero temperature and pressure, we assume structures with tetragonal symmetries and c/a ratios close to one are not stationary and may change to cubic symmetry. Of the structures included in Fig. 2 all of the tetragonal structures either have a c/a ratio of one or are within 20% of that value.

3.1. Predicted structures

From our structural search at zero temperature and zero pressure we have found five ground state structures forming the corresponding convex hull at compositions Li_1 Mg_{13}, Li_1 Mg_2, Li_1 Mg_1, Li_7 Mg_2, Li_{15} Mg_1 and nine metastable structures at compositions Li_1 Mg_3, Li_1 Mg_2, Li_2 Mg_3, Li_3 Mg_4, Li_1 Mg_1, Li_5 Mg_1, Li_6 Mg_1, Li_7 Mg_1, and Li_9 Mg_1. In Table 1 we report the atomic percent Li, the space group by Pearson symbol, the number of atoms in the primitive cell, and the formation energy for each structure.

When compared to the online databases, our methods have recovered all previously reported structures. Li_1 Mg_3, Li_1 Mg_2, Li_1 Mg_1, Li_1 Mg_5, Li_2 Mg_1, Li_3 Mg_1, and Li_5 Mg_1 have been found in the Materials Project database [19–21], the Open Quantum Materials Database [22], and AFLOW [23]. Remarkably, we have also discovered many previously unreported structures. The most interesting of these are those which lie on the convex hull (Li_1 Mg_{13}, Li_7 Mg_2, Li_{15} Mg_1). Their composition, space group, lattice parameters, and DOS at Fermi Energy are given in Table 2.

For the Li_1 Mg_{13} composition, we find a ground state structure of space group *P*1(1). Fig. 4 shows the crystal stucture and the density

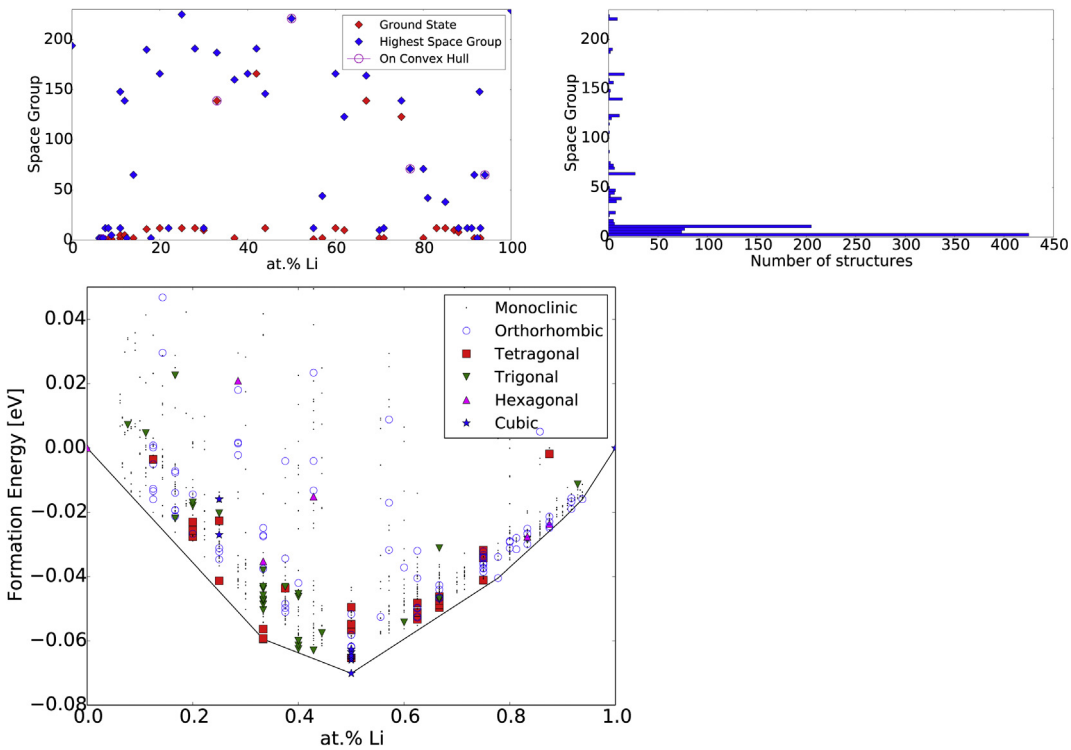

Fig. 2. Space groups found during structure search. Top left: the space group of the highest symmetry structure and the ground state structure vs. at.% Li. Top right: Histogram of the number of stuctures found in each space group with respect to every structure found. Bottom: Convex hull of the Mg-Li binary system with crystal structure indicated by symbols. The left of the plot is pure Li and the right is pure Mg.

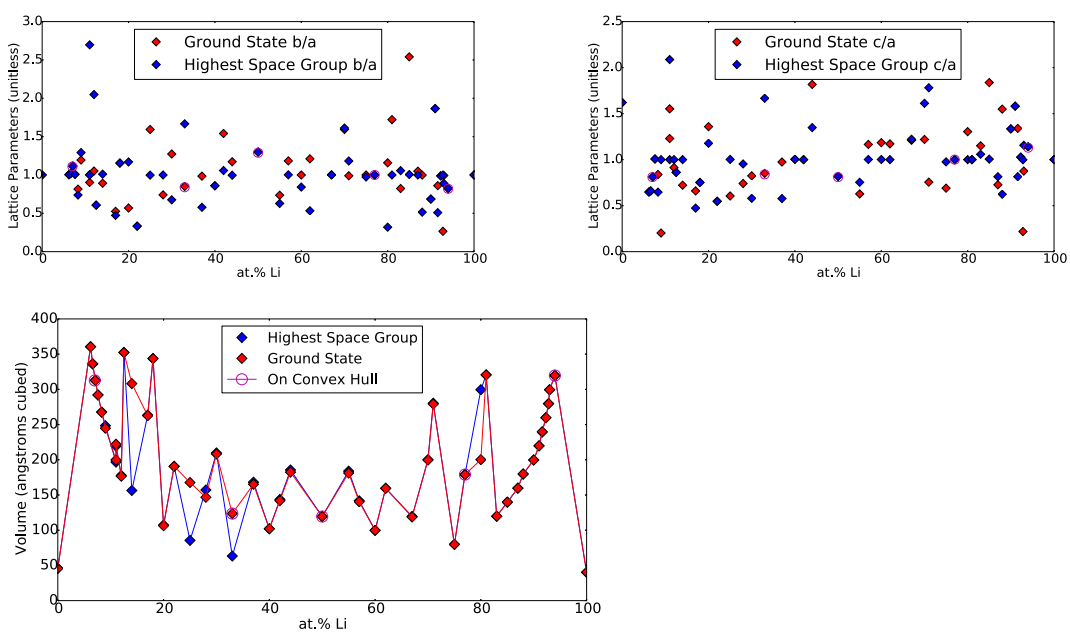

Fig. 3. Top left: b/a ratio with respect to at. % Lithium. Top right: c/a ratio with respect to at. % Lithium. Bottom: volume with respect to at. %Lithium. In all three plots red diamonds indicate the lowest energy state for each composition, blue diamonds represent the highest symmetry state for each composition. (For interpretation of the references to colour in this figure legend, the reader is referred to the web version of this article.)

of states for this structure. The nearest neighbor distance between Mg-Mg atoms, and Mg-Li atoms in this structure is 3.11 Å and 3.10 Å, respectively.

At composition Li_1 Mg_2 we find the ground state structure to be tetragonal and of space group *I*4/*mmm*. Fig. 5 shows the crystal structure and the density of states. The nearest neighbor distance between Mg-Mg atoms, Li-Li atoms, and Mg-Li atoms in this structure is 3.43 Å, 3.43 Å, and 2.94 Å, respectively. For this composition, we also found a low energy hexagonal structure of space group *P*-6*m*2, 24.1 meV per atom above the ground state. Fig. 6 shows the crystal structure and density of states. In the crystal structure the hexagonal pattern can clearly be seen with Mg atoms

Table 2
Space group, lattice parameters in Å, angles in degrees, and DOS at the Fermi Energy for ground state structures.

Composition	Space group	a	b	c	α	β	γ	DOS(Ef)(states/eV)
Li_1 Mg_{13}	*P*1 (1)	6.07	8.09	7.46	114.4	75.9	109.6	2.60
Li_1 Mg_2	*I*4/*mmm* (139)	3.43	3.43	10.53	90	90	90	0.53
Li_1 Mg_1	*Pm*-3*m* (221)	3.42	3.42	3.42	90	90	90	1.06
Li_7 Mg_2	*Immm* (71)	9.67	9.72	3.83	90	90	90	2.23
Li_{15} Mg_1	*Cmmm* (65)	7.45	6.14	7.45	90	110.5	89.9	4.29

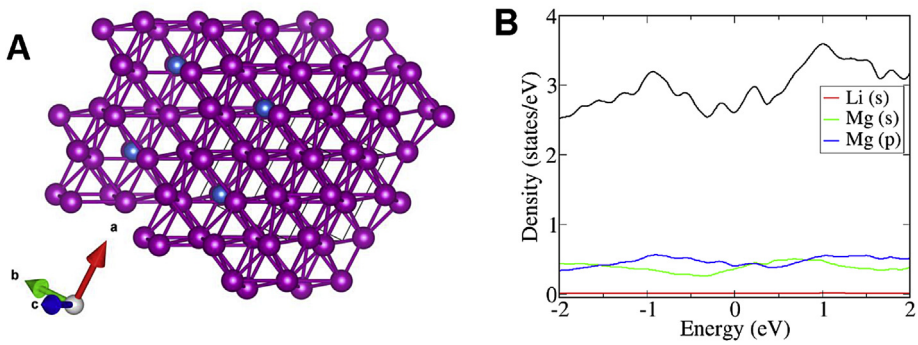

Fig. 4. Li_1 Mg_{13} spacegroup *P*1(1) A) crystal structure, B) density of states (black line indicates total DOS).

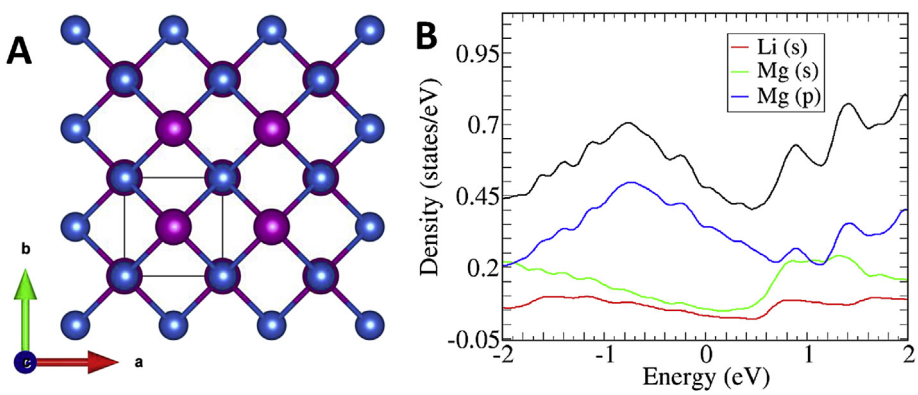

Fig. 5. Li_1 Mg_2 spacegroup *I*4/*mmm*(139) A) crystal structure, B) density of states (black line indicates total DOS).

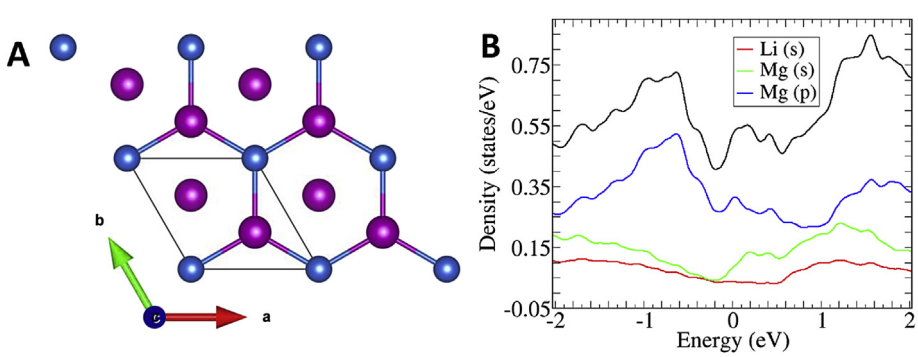

Fig. 6. Li_1 Mg_2 spacegroup *P*-6*m*2(187) A) crystal structure, B) density of states (black line indicates total DOS).

surrounding Li atoms. The nearest neighbor distance between Mg-Mg atoms, Li-Li atoms, and Mg-Li atoms in this structure is 3.22 Å, 4.94 Å, and 2.85 Å, respectively. This is the only structure in which we studied where the phonon dispersion contains negative phonon modes. They appear near the gamma point.

Li_1 Mg_1 is the lowest lying energy structure for the entire LiMg binary system and has been studied extensively [19,20,22,23]. The ground state structure was found to be cubic with space group *Pm*-3*m*. This agrees well with what has been previously reported [3,26,27]. Fig. 7 shows the crystal structure and density of states. The cubic structure is easily recognized. The nearest neighbor distance between Mg-Mg atoms, Li-Li atoms, and Mg-Li atoms in this structure is 3.41 Å, 3.41 Å, and 2.95 Å, respectively. The lowest energy tetragonal structure found for Li_1 Mg_1 is of space group *P*4/

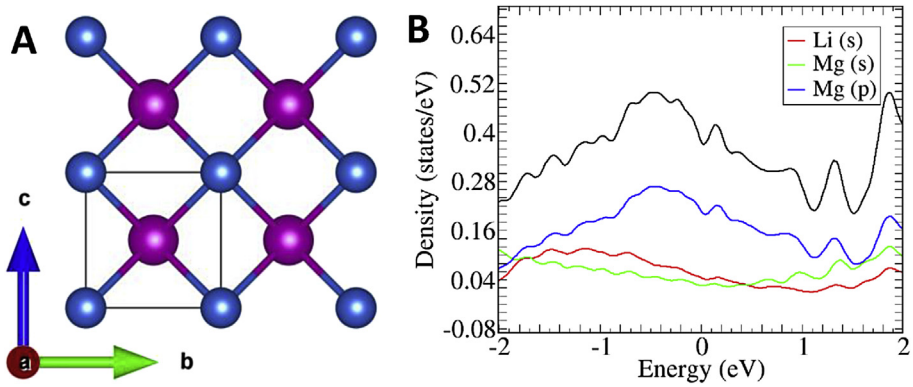

Fig. 7. Li_1 Mg_1 spacegroup *Pm*-3*m*(221) A) crystal structure, B) density of states (black line indicates total DOS).

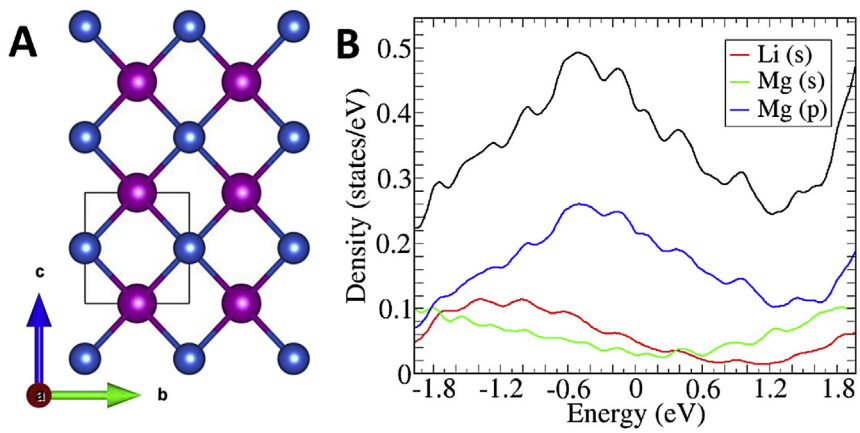

Fig. 8. Li_1 Mg_1 spacegroup *P*4/*mmm*(123) A) crystal structure, B) density of states (black line indicates total DOS).

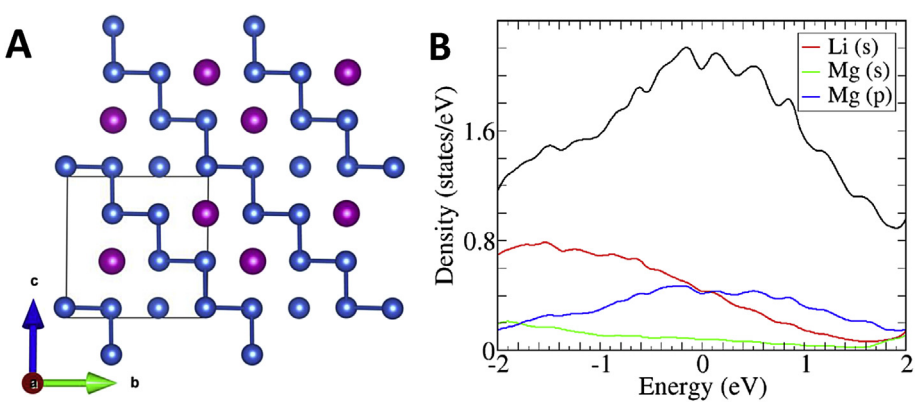

Fig. 9. Li_7 Mg_2 spacegroup *Immm*(71) A) crystal structure and B) density of states (black line indicates total DOS).

mmm and is 4.9 meV per atom above the ground state. Fig. 8 shows the crystal structure and density of states. The nearest neighbor distance between Mg-Mg atoms, Li-Li atoms, and Mg-Li atoms in this structure is 3.36 Å, 3.36 Å, and 2.96 Å, respectively.

There are no previously reported structures for Li_7 Mg_2. We find a ground state structure of space group *Immm*. Fig. 9 shows the crystal structure and density of states. The nearest neighbor distance between Mg-Mg atoms, Li-Li atoms, and Mg-Li atoms in this structure is 3.20 Å, 2.95 Å, and 2.99 Å, respectively.

Structures at composition Li_{15} Mg_1 are previously unreported. As the ground state we find an orthorhombic structure of space group *Cmmm*. Fig. 10 shows the crystal structure and density of states. The nearest neighbor distance between Li-Li atoms and Mg-Li atoms in this structure is 3.02 Å and 3.04 Å.

3.2. Elastic properties

3.2.1. Elastic constants

In order to investigate the elastic properties of these structures, we calculate the elastic stiffness constants C_{ij}. This is done by

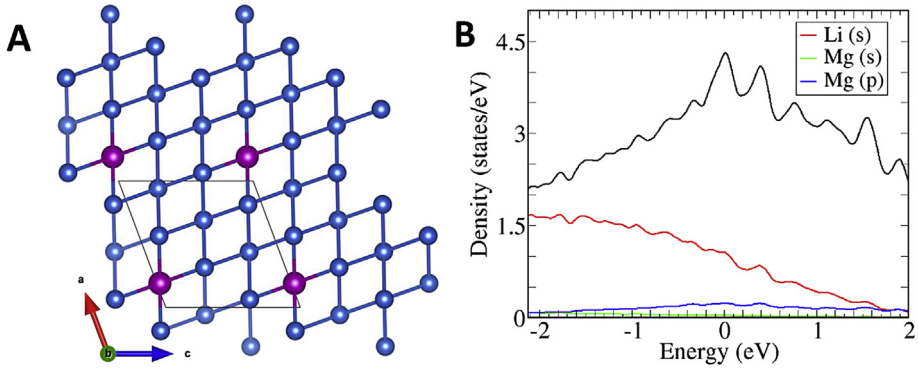

Fig. 10. Li_{15} Mg_1 space group *Cmmm*(65) A) crystal structure and B) density of states (black line indicates total DOS).

Table 3
Computed elastic constants for lowest-energy structures. All values are given in GPa [1] & [2] Ref. [27], [3] Ref. [3].

Structure	C11	C12	C44	C33	C13	C66
Li	15.1	13.3	11.9			
Li [2]	15.1	12.7	11.4			
Li_1 Mg_{13}(1)	57.2	22.2	17.0	58.1	19.6	20.0
Li_1 Mg_3(FCC)(225)	37.3	26.5	0.34			
Li_1 Mg_3(BCC) [2]	41.0	24.0	37			
Li_1 Mg_3(BCC) [1]	41.7	24.8	36.4			
Li_1 Mg_2(187)	62.5	13.3	17.9	83.5	0.60	24.5
Li_1 Mg_2(139)	42.7	21.7	39.7	43.2	21.9	34.0
Li_2 Mg_3(166)	61.6	17.2	22.2	74.7	2.3	
Li_3 Mg_4(191)	42.9	22.4	16.6	74.9	0.82	10.2
Li_1 Mg_1(CCP)(221)	33.0	20.9	18.3			
Li_1 Mg_1(123)	35.7	17.9	26.4	25.7	21.9	22.0
Li_1 Mg_1(BCC) [2]	30.5	19.5	23.4			
Li_1 Mg_1(BCC) [1]	34.1	20.0	26.5			
Li_1 Mg_1(CCP) [3]	37.5	19.7	25.9			
Li_7 Mg_2(71)	20.7	16.7	0.49	31.1	15.8	16.7
Li_5 Mg_1(189)	28.2	16.7	0.42	40.3	0.51	0.57
Li_6 Mg_1(1)						
Li_7 Mg_1(187)	27.1	15.3	0.47	36.4	0.52	0.58
Li_7 Mg_1(FCC) [3]	15.8	16.9	11.7			
Li_9 Mg_1(12)	28.2	10.4	12.7	26.3	0.68	11.9
Li_{15} Mg_1(65)	27.1	8.9	3.8	22.5	8.4	6.6
Mg	56.5	25.1	15.7	56.2	26.6	
Mg [2]	59.5	26.12	16.35	61.55	21.80	

Table 4
Calculated Bulk modulus, Shear modulus, Youngs modulus, Poisson's ratio, and Bulk modulus/Shear modulus (B/G) ratio. [1]. & [2] Ref. [27], [3] Ref. [3].

Structure	Bulk	Shear	Young	Poisson	B/G
Li	13.96	4.77	12.46	0.351	2.92
Li [2]	12.95				
Li [3]	13.3				
Li_1 Mg_{13}(1)	33.16	18.31	46.39	0.267	1.8110
Li_1 Mg_3(FCC)(225)	30.18	18.49	45.04	0.251	1.6322
Li_1 Mg_3(BCC) [2]	30.5	20.4	50.1	0.23	
Li_1 Mg_3(BCC) [1]	29.7				
Li_1 Mg_2(187)	28.75	23.51	55.42	0.17	1.2227
Li_1 Mg_2(139)	28.86	22.71	53.68	0.19	1.2707
Li_3 Mg_4(191)	26.31	15.57	38.98	0.25	1.690
Li_1 Mg_1(CCP)(221)	24.98	11.79	38.50	0.243	2.118
Li_1 Mg_1(123)	24.31	12.94	32.52	0.278	1.878
Li_1 Mg_1(BCC) [2]	24.7	15.7	38.8	0.24	
Li_1 Mg_1(BCC) [1]	23.2				
Li_1 Mg_1(CCP) [3]	25.6	16.9	41.6		1.51
Li_7 Mg_2(71)	17.85	8.14	21.01	0.304	2.1925
Li_5 Mg_1(189)	16.77	6.62	17.52	0.326	2.532
Li_7 Mg_1(187)	16.05	6.71	17.66	0.317	2.3906
Li_7 Mg_1(FCC) [3]	16.6	2.7	8.2		6.15
Li_9 Mg_1(12)	15.40	7.42	19.11	0.293	2.076
Li_{15} Mg_1(65)	14.78	5.26	14.02	0.342	2.80
Mg	36.25	17.51	45.24	0.292	2.070
Mg [2]	34.3				

relating the stresses and strains through the generalized Hooke's law [44].

$$\sigma_{ij} = C_{ijkl}\varepsilon_{kl} \tag{1}$$

where σ_{ij} is the tensile stress and ε_{kl} is the longitudinal strain. Crystal symmetry reduces the number of constants from 81 to 3, 5, 6 and 13 for cubic, hexagonal, tetragonal, and monoclinic respectively. In Table 3 we report these values for each of our structures.

From these we can calculate the macroscopically measurable elastic quantities for materials: Bulk modulus(B), Young's modulus(E), Shear modulus(G), Poisson's ratio(ν), and the B/G ratio. The bulk modulus represents the volume compression and is given by $B = E/3(1-2\nu)$ [44]. Young's modulus represents the stiffness of the system, given by $E = C_{ijkl}$ [44]. The Shear modulus is given by $G = E/2(1+\nu)$ and is used as a measure of elasticity when a shear force is applied [44]. Poisson's ratio is a measure of the expansion of a material when it is compressed in the transverse direction, and is sometimes used as an approximate measure of plastic ductility. It is given by $\nu = -E\ C_{1122}$ [44]. The B/G ratio is a good indicator as to whether a material is brittle or ductile. Values above 1.7, the threshold value, indicates ductility while values below indicate brittleness [45].

Table 4 lists the values of the elastic properties, and in Fig. 11 we plot these properties versus Li concentration. In all these plots, excluding the bulk modulus, we see a jump in the values for Li_1 Mg_2 composition. Both structures show this deviation from the trend. We also see a smaller jump for Li_9 Mg_1. These jumps cannot be accounted for from crystal symmetry, since there are structures with similar, and higher, symmetry such as Li_1 Mg_1. However, as is discussed later, the Li_1 Mg_2 structures exhibit peculiar phonon band dispersions and larger Debye temperatures, and Li_9 Mg_1 has the highest vibrational contribution to the heat capacity.

In general, we see a linear decrease in the bulk, shear, and Young's moduli as Li concentration increases, indicating more elasticity and compressibility in the structures as Li concentration increases. This is in agreement with what has been reported for the bulk modulus [25]. In the compositions Li_1 Mg_1 and Li_1 Mg_2, where there are two structures for each composition, it is interesting to note that the less symmetric tetragonal structures have better values for the shear and Young's moduli. We see this as well in the Poisson's ratio. For the system, the Poisson ratio is generally increasing, indicating an increase of plasticity and metallicity in the

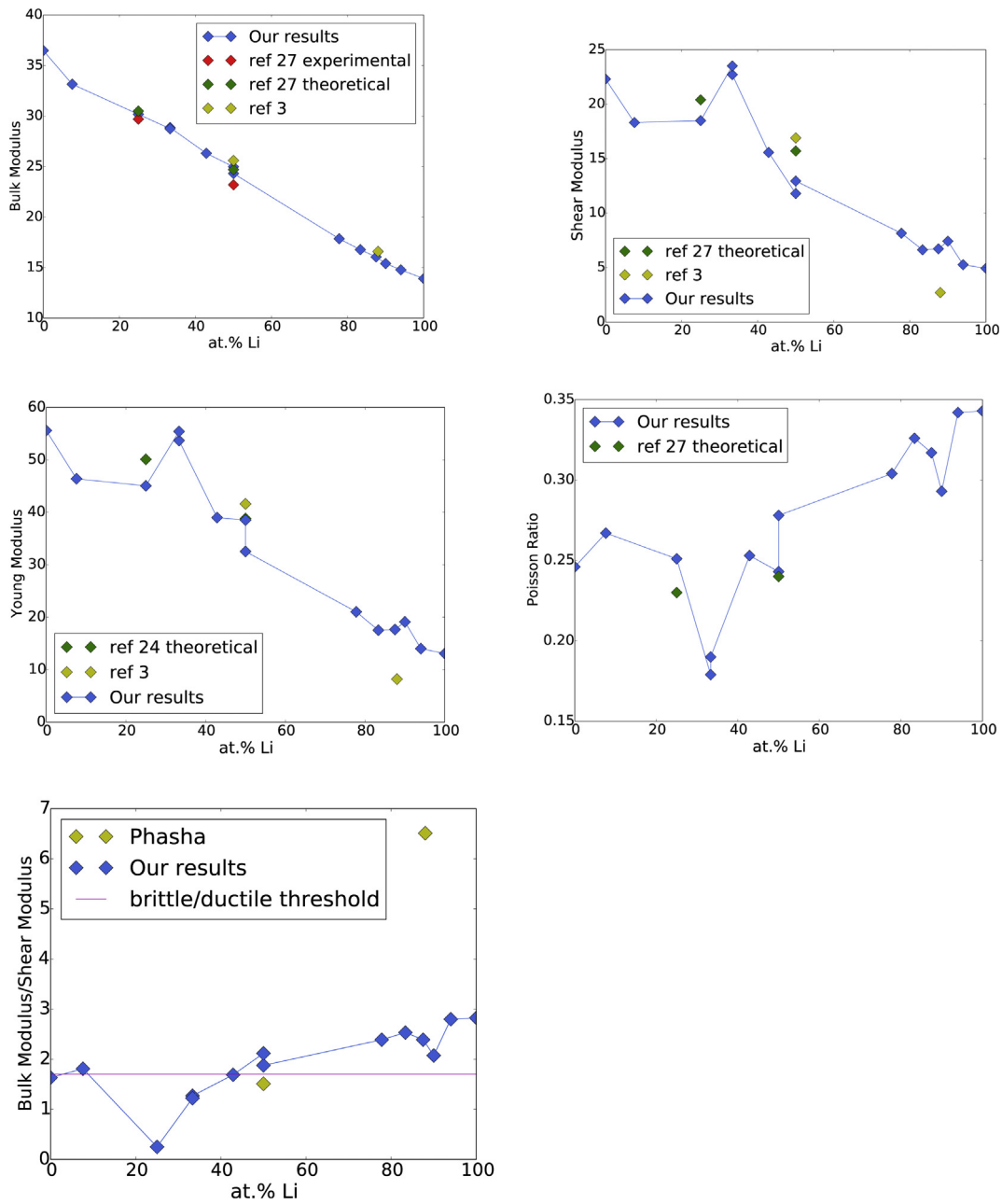

Fig. 11. Elastic constants. ref [27] reports theoretical and experimental results, these are plotted separately. Green diamonds represent theoretical results reported in Ref. [27], red diamonds represent experimental results reported in Ref. [27], yellow diamonds represent results reported in Ref. [3], blue diamonds represent results from this work. (For interpretation of the references to colour in this figure legend, the reader is referred to the web version of this article.)

alloy as Li concentration increases. For alloys with low Li concentrations, the Bulk modulus to Shear modulus ratio lies below the critical value of 1.7, corresponding to brittle behavior. Our results match reasonably well with what has been reported.

Based on the best linear fit line we propose an equation to describe the relationship between the bulk modulus and percent Li concentration. Our data gives

$$B = -0.2342x + 36.387, \tag{2}$$

where x represents Li concentration.

It is well known that at low temperatures the specific heat of crystals follows a T^3 power law. This behavior is attributed to the contribution from the crystal lattice. To find the contribution from vibration of the lattice, we divide the heat capacity by T^3. This is plotted in Fig. 12. We found the heat capacity at 298 K of pure Li and pure Mg to be 22.57 J/mol/K and 23.46 J/mol/K respectively. Experimental results report a heat capacity at 298.15 K of pure Li [46] and pure Mg [47] to both be 20.79 K. Our results match well with this reported data. We report the Debye temperatures of the structures on the convex hull in Table 5. The Debye temperature gives insight into the density, structural stability, and bonding strength of a solid [48]. We note that the Debye model is defined for monoatomic crystals. However, it may be useful to apply it here since we see good agreement between the experimental values for pure Li and pure Mg and our theoretical values.

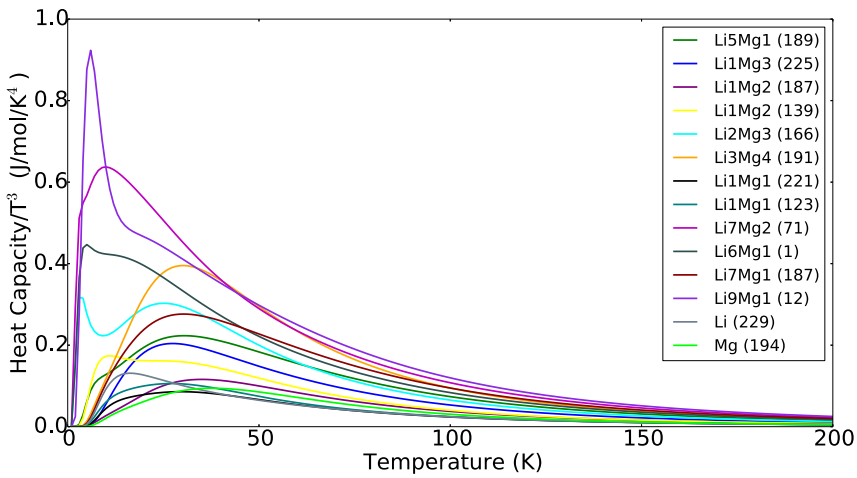

Fig. 12. Heat capacity/T^3 vs Temperature.

4. Lattice thermal conductivity of Li_1Mg_1 and Li_1Mg_2 in the stable configurations

During our study, we found that Li_1 Mg_1 and Li_1 Mg_2 exhibit peculiar phonon band structure, with a clear "phonon band-gap" of around 75 cm^{-1}. In Li_1 Mg_1 such a phonon gap is between acoustic and optical branches while in Li_1 Mg_2 it is within optical branches. A similar phonon band structure has been reported in SnSe, where the authors found two "sets" of twelve phonon branches separated by a phonon gap of 95 cm^{-1} [49]. They reported that, even though optical phonons represent almost 90% of the total number of modes, their contribution to the total thermal conductivity is limited.

Optical phonons are frequently neglected from calculations of thermal conductivity due to their small group velocity with frequencies that typically reside too high with respect to the acoustic branches. Nevertheless, optical phonons provide scattering channels that reduce thermal conductivities like in the cases of silicon and diamond [50,51]. The abnormal phonon band structure in these two compounds represents an opportunity to explore the impact of phonon-gaps in materials and, moreover the differences that can be observed depending on the nature of the branches involved in such phonon-gaps. Our calculations show that, at room temperature, the average thermal conductivity of Li_1 Mg_1 is around four times higher than for Li_1 Mg_2. (Fig. 13 left).

Even though acoustic phonons are mainly responsible for heat transfer, optical phonons provide scattering channels for acoustic branches. From the phonon band structure, we observe that, in Li_1 Mg_2, three optical branches have frequencies very close to the maximum of the acoustic ones. Therefore, we can assume that optical-acoustic phonon-phonon interactions between these two "sets" of phonons will be strong. This is the case of the here mentioned cases of diamond and silicon. By artificially removing acoustic-optic phonon-phonon scattering mechanisms, the thermal conductivity in Si and diamond increases by three and six, respectively. Here we show with practical cases the importance of acoustic-optic phonon interaction as the main factor for reducing acoustic phonon life-times and, therefore, reducing the maximum lattice contribution to the thermal conductivity. We support our conclusion by plotting the cumulative lattice thermal conductivity at 300 K with respect to the maximum allowed mean free path (MFP). This means the value of κ if only phonons with certain MFP are taken into account. Fig. 13 displays the results for two compounds, Li_1 Mg_1 and Li_1 Mg_2. We show, together with the total, the partial cumulative thermal conductivity when only acoustic modes are taken into account. It is clear that in both cases, Li_1 Mg_1 and Li_1 Mg_2, the majority contribution to κ comes from acoustic branches, however, we observe that in Li_1 Mg_2, the total and partial cumulative thermal conductivity split from the beginning, which differs from the behavior of Li_1 Mg_1, where partial and total cumulative κ split near to the converged value. This is a clear indication that optical branches are more important for the phonon transport in Li_1 Mg_2 than in Li_1 Mg_1. We believe that our results could help the development of further materials with improved thermal properties. A good example is in the field of thermoelectric materials, where the thermoelectric performance directly depends of the thermal conductivity.

Table 5
Debye Temperature for compounds on the convex hull in units of K [1]. ref [52], [2] ref [46].

Structure	Debye temperature (K)
Mg	387.2
Mg [1]	330
Li_1 Mg_{13}	346.5
Li_1 Mg_2	382.01
Li_1 Mg_1	344.5
Li_7 Mg_2	296.5
Li_{15} Mg_1	358.9
Li	349.8
Li [2]	344

5. Conclusions

We have performed a systematic study of the Li-Mg binary system considering all compositions from 0 to 100% Mg with up to 16 atoms per unit cell using *ab-initio* density functional theory. We have found five structures belonging to the convex hull, three of these being previously unreported. We have studied their stability in three ways: energetically, thermodynamically, and elastically. We have also calculated the elastic constants and elastic properties, studying how Li content effects these characteristics. We have found that adding low concentrations of Li does not help Mg's inherently low ductility, but does have a positive effect on the other elastic properties. Vibrationally, we find that many of the structures in the system exhibit a gap in the phonon band structure. We have plotted the vibrational contribution to the heat capacity and reported the calculated Debye temperatures. We also find evidence for the role of optical phonon branches as scattering channels

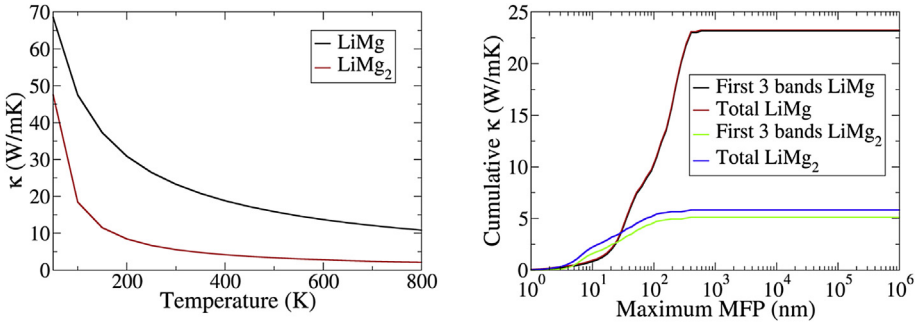

Fig. 13. Left-Temperature dependance of lattice thermal conductivity, For Li_1 Mg_2 the value plotted is the average of the trace. Right-Cumulative κ as a function of the Maximum Mean Free Path (MFP).

which reduce the thermal conductivity of the structure through study of these phonon band gaps.

Acknowledgements

This work used the Extreme Science and Engineering Discovery Environment (XSEDE), which is supported by National Science Foundation grant number OCI-1053575. AHR, SS, GAF and WIH acknowledge the support of DMREF-NSF 1434897 and the Donors of the American Chemical Society Petroleum Research Fund for partial support of this research under contract 54075-ND10.

Appendix A. Supplementary data

Supplementary data related to this article can be found at http://dx.doi.org/10.1016/j.jallcom.2016.08.217.

References

[1] Z. Yang, J. Li, J. Zhang, G. Lorimer, J. Robson, Review on research and development of magnesium alloys, Acta Metall. Sin. Engl. Lett. 21 (5) (2008) 313–328, http://dx.doi.org/10.1016/S1006-7191(08)60054-X. http://www.sciencedirect.com/science/article/pii/S100671910860054X.

[2] J. Trivisonno, C.S. Smith, Elastic constants of lithium-magnesium alloys, Acta Metall. 9 (12) (1961) 1064–1071, http://dx.doi.org/10.1016/0001-6160(61)90175-4. http://www.sciencedirect.com/science/article/pii/0001616061901754.

[3] M. Phasha, P. Ngoepe, H. Chauke, D. Pettifor, D. Nguyen-Mann, Link between structural and mechanical stability of fcc- and bcc-based ordered mgli alloys, Intermetallics 18 (11) (2010) 2083–2089, http://dx.doi.org/10.1016/j.intermet.2010.06.015. http://www.sciencedirect.com/science/article/pii/S0966979510002736.

[4] I. Shin, E.A. Carter, First-principles simulations of plasticity in body-centered-cubic magnesiumlithium alloys, Acta Mater. 64 (2014) 198–207, http://dx.doi.org/10.1016/j.actamat.2013.10.030. http://www.sciencedirect.com/science/article/pii/S1359645413007933.

[5] B.R. Sahu, Electronic structure and bonding of ultralight limg, Mater. Sci. Eng. B 49 (1) (1997) 74–78. http://wvu.summon.serialssolutions.com/2.0.0/link/0/eLvHCXMwpV1LSwMxEA7qSRHfYn1ADh70sO1uss0mRyktHvQgKuhpSbJJW5C2SIt_38mjLx8oel1ms9mZ8M0kmfkGIUrqafIBE2AVAVymHPYs4IENLBKjla2YFJppyfQybXcojYlJltETBlT32B2fNKJuG6N-v3GfCue80kIUDoG5K_9tstwled3ROX94Fu8VQDhx0vOanjCCf3ghiks_SMK_81ZfOCnvkDrbqLcw91mbhbfQzOEz1eM__nAHbcWgFV8FuV20YgZ7aGOBynAf0fasnw4OnLSTV4PloMJq6Atn8NDiyYs_V-n2xvimf9s9QI-d9kPrOokNGRJNXNa_AnxwlbMqI0yB-QgziiljraogcIRIQDq-ecZcA2NZ5cKmlhltRUUyqYnW9BBtSpe4Pxj7Ar_qCGHNOMl5rqyGrSrEX4IKy7k0lDYB_5qkhupTC5SjQMBRzjPTQCWl00kZrtEZL3kN8amdyiXNluAkfnr1fNGus-85auDi6TnLCx8y11D2G7FWJFl35ALj47_P6gStB85cd-5zitbAhuYMrcKSegcQHf8b.

[6] B. Mordike, T. Ebert, Magnesium: properties applications potential, Mater. Sci. Eng. A 302 (1) (2001) 37–45, http://dx.doi.org/10.1016/S0921-5093(00)01351-4. http://www.sciencedirect.com/science/article/pii/S0921509300013514.

[7] G.S. Cole, Issues that influence magnesium's use in the automotive industry, Mater. Sci. Forum 419–422 (2003) 43–50.

[8] E. Aghion, B. Bronfin, D. Eliezer, The role of the magnesium industry in protecting the environment, J. Mater. Process. Technol. 117 (3) (2001) 381–385, http://dx.doi.org/10.1016/S0924-0136(01)00779-8 containing keynote papers presented at the proceedings of THERMEC'2000, the International conference on Processing and manufacturing of Advanced Materials, http://www.sciencedirect.com/science/article/pii/S0924013601007798.

[9] Z. Wu, W. Curtin, The origins of high hardening and low ductility in magnesium, Nature 526 (7571) (2015), 62–62.

[10] A. Luque, M. Ghazisaeidi, W.A. Curtin, Deformation modes in magnesium (0001) and single crystals: simulations versus experiments, Model. Simul. Mater. Sci. Eng. 21 (4) (2013) 045010. http://stacks.iop.org/0965-0393/21/i=4/a=045010.

[11] F. Kang, Z. Li, J.T. Wang, P. Cheng, H.Y. Wu, The activation of c+a non-basal slip in magnesium alloys, J. Mater. Sci. 47 (22) (2012) 7854–7859, http://dx.doi.org/10.1007/s10853-012-6344-z.

[12] J. Geng, M. Chisholm, R. Mishra, K. Kumar, The structure of c + a type dislocation loops in magnesium, Philos. Mag. Lett. 94 (6) (2014) 377–386.

[13] S. Sandlbes, Z. Pei, M. Frik, L.-F. Zhu, F. Wang, S. Zaefferer, D. Raabe, J. Neugebauer, Ductility improvement of mg alloys by solid solution: ab initio modeling, synthesis and mechanical properties, Acta Mater. 70 (2014) 92–104, http://dx.doi.org/10.1016/j.actamat.2014.02.011. http://www.sciencedirect.com/science/article/pii/S1359645414000949.

[14] K. Chen, K.P. Boyle, Elastic properties, thermal expansion coefficients, and electronic structures of mg and mg-based alloys, Metallurgical Mater. Trans. A 40 (11) (2009) 2751–2760, http://dx.doi.org/10.1007/s11661-009-9954-6.

[15] F. Wang, S. Sandlbes, M. Diehl, L. Sharma, F. Roters, D. Raabe, In situ observation of collective grain-scale mechanics in mg and mgrare earth alloys, Acta Mater. 80 (2014) 77–93, http://dx.doi.org/10.1016/j.actamat.2014.07.048. http://www.sciencedirect.com/science/article/pii/S1359645414005667.

[16] Z. Pei, M. Frik, S. Sandlbes, R. Nazarov, B. Svendsen, D. Raabe, J. Neugebauer, Rapid theory-guided prototyping of ductile mg alloys: from binary to multicomponent materials, New J. Phys. 17 (9) (2015) 093009. http://stacks.iop.org/1367-2630/17/i=9/a=093009.

[17] W.A. Counts, M. Frik, D. Raabe, J. Neugebauer, Using ab initio calculations in designing bcc mglix alloys for ultra-lightweight applications, Adv. Eng. Mater. 12 (12) (2010) 1198–1205, http://dx.doi.org/10.1002/adem.201000225.

[18] C.S. Barrett, A low temperature transformation in lithium, Phys. Rev. 72 (3) (1947), 245–245, http://wvu.summon.serialssolutions.com/2.0.0/link/0/eLvHCXMwjV09T8MwED0BEhIS4hvxKXljQClx7MT2WCEqhk5VBrbIXxEdSBGk9O9zjkNV2gEGb7YUPSV5d7537wBYNkiTtX-CMFZh4mxw2ToUY3KV5l4KoVzQLfjftt3L64-1gj5N2UMQRk7810Bkg4yH5nKOHNr1jUyW1QOueHRfZjTBfOKlN2vcPL5CRiusMjqE5filKLOOkpJFnMiw6df452MewUEfX5JhfCGOYcs3J7Db6Tzt5yncD8l4tiClx2g5uimTciV0nTVk2pDxtH2dzt_OoBw9lY_PST8vIbFFsBV2LLc5M8bUVCqRF05jsOMdV8hBrtZGIFlhPhocBKU1phCeMaNriR91kTnGzmFfB1l903btd-4CiLQ-NQgj9UJzL6UWNIzmEIXXnlprLuHuB8DqPdpjVF1akbKqh6ASWYUQXP175zXsUcVFVNndwE77Mfe3sI3ofwMvW6l7.

[19] S.P. Ong, L. Wang, B. Kang, G. Ceder, Li-Fe-P-O2 phase diagram from first principles calculations, Chem. Mater. 20 (5) (2008) 1798–1807, http://dx.doi.org/10.1021/cm702327g.

[20] A. Jain, G. Hautier, S. Ong, C. Moore, C. Fischer, K. Persson, G. Ceder, Formation enthalpies by mixing GGA and GGA + U calculations, Phys. Rev. B 84 (4) (2011) 045115, http://dx.doi.org/10.1103/PhysRevB.84.045115. http://link.aps.org/doi/10.1103/PhysRevB.84.045115.

[21] A. Jain, S.P. Ong, G. Hautier, W. Chen, W.D. Richards, S. Dacek, S. Cholia, D. Gunter, D. Skinner, G. Ceder, K. a. Persson, The Materials Project: a materials genome approach to accelerating materials innovation, Apl. Mater. 1 (1) (2013) 011002, http://dx.doi.org/10.1063/1.4812323. http://link.aip.org/link/AMPADS/v1/i1/p011002/s1/&Agg=doi.

[22] J. Saal, S. Kirklin, M. Aykol, B. Meredig, C. Wolverton, Materials design and discovery with high-throughput density functional theory: the open quantum materials database (oqmd), JOM 65 (11) (2013) 1501–1509, http://dx.doi.org/10.1007/s11837-013-0755-4.

[23] S. Curtarolo, W. Setyawan, G.L. Hart, M. Jahnatek, R.V. Chepulskii, R.H. Taylor, S. Wang, J. Xue, K. Yang, O. Levy, M.J. Mehl, H.T. Stokes, D.O. Demchenko, D. Morgan, Aflow: an automatic framework for high-throughput materials

discovery, Comput. Mater. Sci. 58 (2012) 218–226, http://dx.doi.org/10.1016/j.commatsci.2012.02.005.
[24] T. Uesugi, M. Kohyama, M. Kohzu, K. Higashi, Ab initio calculation on the structure and elastic properties of a magnesium-lithium alloy, Mater. Trans. 42 (7) (2001) 1167–1171, http://dx.doi.org/10.2320/matertrans.42.1167.
[25] W. Counts, M. Frik, D. Raabe, J. Neugebauer, Using ab initio calculations in designing bcc mgli alloys for ultra-lightweight applications, Acta Mater. 57 (1) (2009) 69–76, http://dx.doi.org/10.1016/j.actamat.2008.08.037. http://www.sciencedirect.com/science/article/pii/S1359645408006253.
[26] R.H. Taylor, S. Curtarolo, G.L.W. Hart, Ordered magnesium-lithium alloys: first-principles predictions, Phys. Rev. B 81 (2010) 024112, http://dx.doi.org/10.1103/PhysRevB.81.024112. http://link.aps.org/doi/10.1103/PhysRevB.81.024112.
[27] C.P. Liang, H.R. Gong, Phase stability, mechanical property, and electronic structure of mgli system, J. Alloys Compd. 489 (1) (2010) 130–135, http://dx.doi.org/10.1016/j.jallcom.2009.09.032. http://www.sciencedirect.com/science/article/pii/S0925838809017769.
[28] M. Phasha, P. Ngoepe, An alternative dft-based model for calculating structural and elastic properties of random binary hcp, {FCC} and {BCC} alloys: mgli system as test case, Intermetallics 21 (1) (2012) 88–96, http://dx.doi.org/10.1016/j.intermet.2011.09.015. http://www.sciencedirect.com/science/article/pii/S0966979511003165.
[29] S. Goedecker, Minima hopping: an efficient search method for the global minimum of the potential energy surface of complex molecular systems, J. Chem. Phys. 120 (21) (2004) 9911–9917, http://dx.doi.org/10.1063/1.1724816. http://scitation.aip.org/content/aip/journal/jcp/120/21/10.1063/1.1724816.
[30] M. Amsler, S. Goedecker, Crystal structure prediction using the minima hopping method, J. Chem. Phys. 133(22). http://dx.doi.org/10.1063/1.3512900. URL http://scitation.aip.org/content/aip/journal/jcp/133/22/10.1063/1.3512900.
[31] M.K. Amsler, Crystal Structure Prediction Based on Density Functional Theory, Ph.D. thesis, University Basel, 1984, http://dx.doi.org/10.5451/unibas-006266444, http://edoc.unibas.ch/33436/.
[32] G. Kresse, J. Furthmüller, Efficient iterative schemes for *ab initio* total-energy calculations using a plane-wave basis set, Phys. Rev. B 54 (1996) 11169–11186, http://dx.doi.org/10.1103/PhysRevB.54.11169.
[33] G. Kresse, D. Joubert, From ultrasoft pseudopotentials to the projector augmented-wave method, Phys. Rev. B 59 (1999) 1758–1775, http://dx.doi.org/10.1103/PhysRevB.59.1758.
[34] J.P. Perdew, K. Burke, M. Ernzerhof, Generalized gradient approximation made simple, Phys. Rev. Lett. 77 (1996) 3865–3868, http://dx.doi.org/10.1103/PhysRevLett.77.3865. http://link.aps.org/doi/10.1103/PhysRevLett.77.3865.
[35] A. Togo, I. Tanaka, First principles phonon calculations in materials science, Scr. Mater 108 (2015) 1–5.
[36] A. Togo, F. Oba, I. Tanaka, First-principles calculations of the ferroelastic transition between rutile-type and $cacl_2$-type sio_2 at high pressures, Phys. Rev. B 78 (2008) 134106–134114.
[37] P. Giannozzi, S. Baroni, N. Bonini, M. Calandra, R. Car, C. Cavazzoni, D. Ceresoli, G.L. Chiarotti, M. Cococcioni, I. Dabo, A. Dal Corso, S. de Gironcoli, S. Fabris, G. Fratesi, R. Gebauer, U. Gerstmann, C. Gougoussis, A. Kokalj, M. Lazzeri, L. Martin-Samos, N. Marzari, F. Mauri, R. Mazzarello, S. Paolini, A. Pasquarello, L. Paulatto, C. Sbraccia, S. Scandolo, G. Sclauzero, A.P. Seitsonen, A. Smogunov, P. Umari, R.M. Wentzcovitch, Quantum espresso: a modular and open-source software project for quantum simulations of materials, J. Phys. Condens. Matter 21 (39) (2009) 395502, 19pp, http://www.quantum-espresso.org.
[38] W. Li, L. Lindsay, D.A. Broido, D.A. Stewart, N. Mingo, Thermal conductivity of bulk and nanowire mg2sixsn1-x alloys from first principles, Phys. Rev. B 86 (2012) 174307.
[39] W. Li, J. Carrete, N.A. Katcho, N. Mingo, ShengBTE: a solver of the Boltzmann transport equation for phonons, Comp. Phys. Commun. 185 (2014) 17471758, http://dx.doi.org/10.1016/j.cpc.2014.02.015.
[40] F. Mouhat, F. Coudert, Necessary and sufficient elastic stability conditions in various crystal systems, Phys. Rev. B 90(22). URL http://wvu.summon.serialssolutions.com/2.0.0/link/0/eLvHCXMwlV1LS8NAEB5UEATxLdYH7MGbtu4rm-SoxeJFEVHwFjb7AEGiNG2l_959JKVqD_W-G5bJkpkv833fADDaw91f3wQqc5JkyqrSeECQMyvS1BlrqTZJGn5_zNl2w-Xihj7B7MoTI5_M5KaX455PP8ElAvhxzaw-9dZB4HnPHY6vYSMUNIKZhY-4kdSWpCAQrIZbEM71bVhX0emyVcc1PDXxnGp0-_AVlN6out4V3ZhxVR7sB4ooKreh8cH4yUDcjhFstKoHgdzCZeTkHEVttuDXCEZqLRT5EC0jlwv9FahicPbH-MaqeHULXlH0R26PoCXwe1z_67bzFvoSiJy2hW2ZEpinVMstLVSmtJmXLoawKUsYxPCPHgxgqjM8gwrI6QDlELTTMsyzTg7hE3pefnVKOj39BEgI6yhXKUskdh7scmMSMWUUikvqdCyAxdt5IvP6K9RBFyCWdEGq8hxEYPVgfP5lzPbEWx23B1IvfAI0w6QZZb1Gxd0r_4fHf_rICew4SonHnktp7A2Go7NGay6q_AN2InfZA.
[41] A.R. Wazzan, L.B. Robinson, Elastic constants of magnesium-lithium alloys, Phys. Rev. 155 (1967) 586–594, http://dx.doi.org/10.1103/PhysRev.155.586. http://link.aps.org/doi/10.1103/PhysRev.155.586.
[42] F. Herbstein, B. Averbach, The structure of lithium-magnesium solid solutions-i, Acta Metall. 4.
[43] D. Levinson, On the lattice parameter of mg-li beta alloys, Acta Metall. 3.
[44] J.F. Nye, Physical Properties of Crystals: Their Representation by Tensors and Matrices, Clarendon Press, Oxford, 1957. http://wvu.summon.serialssolutions.com/2.0.0/link/0/eLvHCXMwY2AwNtIz0EUrE8wM0lITU83MQfWZWaJxikGaRaJ5kmVamqVZoqUR-FoypGO7GWCnQuSC7ksA9pBzKvPA07x65ZBLEfBM0FiaAitxZgZmoE2grliQEbDSKldd7AOuNNwEGVhAGwmEGJhS84QZOJ1hN6sJM3AjHQIowiAfAA0qhQLQwHgR6IRThfw0heSiSmDLLadYlEHSzTXE2UMXaH48dLQlHuIAIzEG3kTQEvW8EvBWthQJBoUkk5SUpEQLkxQj42Rg8WRkmZhknGhgnpqUbJCcmGKYLMkghGmQFDZBaQYuIMMcMhIgw8CaBnRMqizYnwAjxG0G.
[45] S. Pugh, Xcii. relations between the elastic moduli and the plastic properties of polycrystalline pure metals, Lond. Edinb. Dublin Philosophical Mag. J. Sci. 45 (367) (1954) 823–843, http://dx.doi.org/10.1080/14786440808520496.
[46] J. Chase, M.W., C.Davies, J.Downey, J.R., D.Frurip, R.McDonald, A.Syverud, Janaf thermochemical tables third edition, J. Phys. Chem. Reference Data 14.
[47] L. Gurvich, Reference books and data banks on the thermodynamic properties of individual substances, Pure Appl. Chem. 61 (2009) 1027–1031.
[48] F. Han, Modern Course in the Quantum Theory of Solids, WSPC, Singapore, SG, 2012.
[49] J. Carrete, N. Mingo, S. Curtarolo, Low thermal conductivity and triaxial phononic anisotropy of snse, Appl. Phys. Lett. 105 (10) (2014), http://dx.doi.org/10.1063/1.4895770.
[50] N. Mingo, D. Stewart, D. Broido, L. Lindsay, W. Li, Ab initio thermal transport, in: S.L. Shind, G.P. Srivastava (Eds.), Length-scale Dependent Phonon Interactions, Vol. 128 of Topics in Applied Physics, Springer, 2014, pp. 137–173, http://dx.doi.org/10.1007/978-1-4614-8651-0_5.
[51] C. Ho, R.W. Powell, P. Liley, Thermal conductivity of the elements: a comprehensive review, J. Phys. Chem. Reference Data 3 (1974) 1–796.
[52] J. Filby, D. Martin, Proc. Roy. Soc. Lond. Ser. 187.